EurJIC
European Journal of Inorganic Chemistry

Full Paper
doi.org/10.1002/ejic.202000415

SOD Mimics

Cobalt(II), Zinc(II), Iron(III), and Copper(II) Complexes Bearing Positively Charged Quaternary Ammonium Functionalities: Synthesis, Characterization, Electrochemical Behavior, and SOD Activity

Marko Stojičkov,[a][‡] Sabrina Sturm,[b][‡] Božidar Čobeljić,[a] Andrej Pevec,[c] Mima Jevtović,[a] Andreas Scheitler,[b] Dušanka Radanović,[d] Laura Senft,[b] Iztok Turel,[c] Katarina Andjelković,[a] Matthias Miehlich,[b] Karsten Meyer,[b] and Ivana Ivanović-Burmazović*[b,e]

Abstract: We have synthesized and characterized Co(II) (**1**), Zn(II) (**2**), Fe(III) (**3**) and Cu(II) (**4**) complexes of 2,2′-[2,6-pyridinediylbis(ethylidyne-1-hydrazinyl-2-ylidene)]bis[*N*,*N*,*N*-trimethyl-2-oxoethanaminium] dichloride ($\mathbf{H_2L}Cl_2$) by NMR, IR, and X-Band EPR spectroscopy, respectively, as well as by single-crystal X-ray structural analysis. $\mathbf{H_2L}Cl_2$ belongs to the class of diacetylpyridine bis(hydrazone) ligands and bears two positively charged quaternary ammonium functionalities. The complexes **1**–**3** possess a pentagonal-bipyramidal geometry, whereas **4** has square-pyramidal geometry. Redox reactivity and SOD activity of the complexes was studied by means of electrochemical measurements in aqueous-buffer and DMF or DMSO solutions, respectively, as well as by stopped-flow measurements. Complexes **1**–**3** do not have SOD activity, whereas **4** exhibits a high catalytic rate constant for the superoxide dismutation, $k_{cat} = 1.73 \times 10^7$ M^{-1} s^{-1} (in MOPS buffer solution of pH = 7.4). The results were discussed in terms of complex redox potentials, electrostatic interactions and their spatial distribution, kinetic lability of metal centers, and stability of peroxo intermediates, respectively.

Introduction

Diacetylpyridine bis(hydrazone) ligands and their derivatives represent a versatile class of polydentate ligands that are suitable for tuning of coordination spheres around metal centers in order to modulate the structural and electronic properties of the corresponding complexes for multi-purpose applications.[1–3] This type of chelators is particularly suitable for the synthesis of the complexes with uncommon geometries, such as seven-coordinate 3*d* metal complexes in a pentagonal bipyramidal (PBP) coordination environment.[2–4] The field of their application is quite broad and includes the design of coordination polymers,[5] supramolecular assemblies, and nanostructures,[6] nanomagnets,[7] as well as investigations of spin-crossover and magnetic relaxation processes,[8,9] photo-induced transformations,[10] and magnetic anisotropy.[11–13] Even more, the PBP 3*d* metal complexes of diacetylpyridine bis(hydrazone) ligands also emerged as bioactive compounds[14–16] and superoxide dismutase (SOD) mimetics.[17] Importantly, related PBP complexes of pyridine-containing pentaazamacrocycles belong to one of the most prominent classes of SOD mimetics that entered clinical trials, with a representative complex that exceeds the SOD activity of the natural enzyme.[18–22] Another important class of SOD mimetics is based on porphyrin complexes, which prominent feature is that they bear positively charged groups on the ring periphery.[23–26] The structure-activity relationship studies on porphyrin systems revealed that metalloporphyrins without the positively charged groups are SOD inactive and that the spatial distribution of the positive charge significantly affects the SOD activity.[23–26] This is an important example of how ligand derivatization with positively charged side chains facilitates the interaction with superoxide, similar to what is found in the enzymatic systems.[27] The related studies on non-porphyrin

[a] *M. Stojičkov, B. Čobeljić, M. Jevtović, Prof. Dr. K. Andjelković*
Faculty of Chemistry, University of Belgrade,
Studentski trg 12-16, 11000 Belgrade, Serbia
https://www.chem.bg.ac.rs/index-en.html
[b] *S. Sturm, A. Scheitler, L. Senft, M. Miehlich, Prof. Dr. K. Meyer, Prof. Dr. I. Ivanović-Burmazović*
Department of Chemistry and Pharmacy, Friedrich-Alexander University Erlangen-Nürnberg,
Egerlandstr. 1, 91058, Erlangen, Germany
https://www.chemistry.nat.fau.eu/
[c] *A. Pevec, Prof. Dr. I. Turel*
Faculty of Chemistry and Chemical Technology, University of Ljubljana,
Večna pot 113, 1000 Ljubljana, Slovenia
http://ruturel.fkkt.uni-lj.si/
[d] *Dr. D. Radanović*
Institute of Chemistry, Technology and Metallurgy, University of Belgrade,
Njegoševa 12, P.O. Box 815, 11000 Belgrade, Serbia
https://www.ihtm.bg.ac.rs/en/
[e] *Prof. Dr. I. Ivanović-Burmazović*
Department Chemie, Ludwigs-Maximilians-Universität,
Butenandtstraße 5-13, 81377 München, Germany
E-mail: Ivana.Ivanovic-Burmazovic@cup.uni-muenchen.de
https://www.cup.lmu.de/de/departments/chemie/
[‡] These authors contributed equally to this work.
Supporting information and ORCID(s) from the author(s) for this article are available on the WWW under https://doi.org/10.1002/ejic.202000415.

Part of a joint Special Collection on Inorganic Enzyme Mimics.

systems bearing positively charged groups are rather rare in the literature. Metallocorroles are one of such rare examples.[28] A derivative of the pentaazamacrocyclic complexes with one lipophilic triphenylphosphonium cation attached to the pyridine moiety, did not show an enhancement of the complex SOD activity.[22] Since the attached positively charged group was not in a close proximity to the metal center, a prominent influence on the superoxide binding and the redox reactivity of the complex was not observed. The complex is, however, important due to its mitochondria-targeting property.[22]

The acyclic complexes with increased number of positive arginine residues at the backbone of the ligand were recently studied regarding potential tuning of their SOD activity.[29] Indeed, the introduction of one arginine-residue had a small but still observable enhancing effect (k_{cat} = 5.0×10^6 M^{-1} s^{-1} for the unsubstituted complex vs. k_{cat} = 6.6×10^6 M^{-1} s^{-1} for mono-arginine complex). A stronger effect was not observed due to the prominent distance between the metal center and the charged group. Introduction of the additional charges on longer chains did not cause any further effect.[29] Principles of host–guest chemistry were also used to introduce a positively charged guest molecule in close proximity to an SOD active copper metal center. By tuning spatial orientation of the positively charged guest (i.e. facing towards or away from copper binding site) an increased SOD-like activity could be achieved, when external positive charge and copper met.[30] These results demonstrate that structure of the complex and position of the charged groups, as well as possible electronic communication with the metal center are crucial for tuning the SOD activity of the mimetic systems.

In that line, we have been studied PBP 3*d* metal complexes of diacetylpyridine bis(hydrazone) ligands,[2,17,31,32] as well as hydrazine complexes with positively charged quaternary ammonium groups from the Girard's T reagent.[33] Motivated by above discussed aspects of such complexes, we have herein synthesized and characterized Co(II), Zn(II), Fe(III) and Cu(II) complexes of 2,2′-[2,6-pyridinediylbis(ethylidyne-1-hydrazinyl-2-ylidene)]bis[*N*,*N*,*N*-trimethyl-2-oxoethanaminium] dichloride (**H_2L**Cl_2). Besides their single-crystal X-ray diffraction (sc-XRD), NMR and EPR analysis, we have also studied their electrochemical behavior and SOD activity. The obtained results enabled us to gain new insights into the effects of positively charged functionalities on the redox properties and potential SOD catalysis of the diacetylpyridine bis(hydrazone) complexes.

Results and Discussion

Synthesis of Complexes

The ligand {2,2′-[2,6-pyridinediylbis(ethylidyne-1-hydrazinyl-2-ylidene)]bis [*N*,*N*,*N*-trimethyl-2-oxoethanaminium] dichloride tetrahydrate} (**H_2L**Cl_2·$4H_2O$) was synthesized in the reaction of 2,6-diacetylpyridine and Girard's T reagent as described previously[34] and used in the synthesis of complexes without further purification. Complexes of Co(II) (**1**), Zn(II) (**2**), Fe(III) (**3**) and Cu(II) (**4**) with **H_2L**Cl_2 were prepared through a direct reaction between the ligand and the corresponding metal salt in the presence of NaOCN or NaN_3 in 1:1:4 molar ratio (Scheme 1). In all complexes the bishydrazone ligand is coordinated in double deprotonated form due to the presence of basic NaOCN or NaN_3 in the reaction solutions. The overall charge of the coordinated ligand remains zero due to the presence of two quaternary ammonium moieties. By way of comparison, deprotonation of the bishydrazone ligand is not observed in the case of analogues Co(II)[35] and Zn(II)[36] complexes, when an excess of NH_4SCN was used instead of NaOCN or NaN_3. In these complexes binding of anionic SCN^- to the axial positions completes their pentagonal-bipyramidal coordination sphere.[34–36]

IR Spectra

The IR spectroscopy data (solid state and solution spectra are presented in Figure S1) confirm that the H_2LCl_2 ligand is coordinated in a doubly deprotonated form, since the ν(N–H) band is absent. Presence of a weak, sharp peak at 3573 cm^{-1} in the spectrum of **1**, and 3566 cm^{-1} in the spectrum of **2**, point to the coordination of water ν(O–H). In the IR spectra of **3** a strong band at 2034 cm^{-1} originates from coordinated N_3^-. Instead of the ν(C=O) band at 1709 cm^{-1}, observed in the spectrum of the ligand **H_2L**Cl_2, the new bands at 1649 cm^{-1}, 1647 cm^{-1}, 1613 cm^{-1} and 1651 cm^{-1} appeared in the spectra of **1**, **2**, **3** and **4** complexes, respectively, being assigned to the ν($^-$O–C=N) vibrations of the deprotonated hydrazine moieties. Coordination of azomethine nitrogen atoms results in the shift of ν(C=N) band from 1630 cm^{-1} in the spectrum of the ligand **H_2L**Cl_2 to 1570 cm^{-1}, 1572 cm^{-1}, 1559 cm^{-1}and 1609 cm^{-1} in the spectra of complexes **1**, **2**, **3** and **4**, respectively. Appearance of a strong band at 1051 cm^{-1}, 1053 cm^{-1}, 1054 cm^{-1} and 1037 cm^{-1}in the spectra of complexes **1**, **2**, **3** and **4**, respectively, refer to the tetrafluoroborate ion.

NMR Spectra of Ligand and Zn(II) Complex

Absence of the H–N signal in the ^{1}H NMR spectra of the Zn(II) complex (**2**), indicates that the ligand is coordinated in its doubly deprotonated form (Table S1, assignment of C atoms corresponds to that given in Scheme 1). Coordination of the ligand through carbonyl oxygen atoms results in an upfield shift of the methylene (H–C7) signals in the ^{1}H NMR spectrum of **2**. An upfield shift of the H–C5 hydrogen signal indicates coordination of the azomethine nitrogen atoms in **2**. Due to coordination via pyridine nitrogen atom, the signals of carbon atoms from pyridine ring in the ^{13}C NMR spectra (Table S2) are reversed (the signal of C1 is shifted upfield and that of C3 is shifted downfield). Coordination of the azomethine nitrogen atom results in an upfield shift of the signals for azomethine C4 and methyl C5 carbon atoms. Coordination of the carbonyl oxygen atom causes an upfield shift of signals of C6 and C7 atoms. Thus, the ^{13}C NMR spectra indicate that pyridine and two azomethine nitrogen atoms, as well as two carbonyl oxygen atoms represent coordination sites of the pentadentate ligand.

Description of the Crystal Structures

Crystals of **1**–**4** suitable for X-ray diffraction analyses were prepared by slow evaporation of solvent at room temperature. Se-

Full Paper
doi.org/10.1002/ejic.202000415

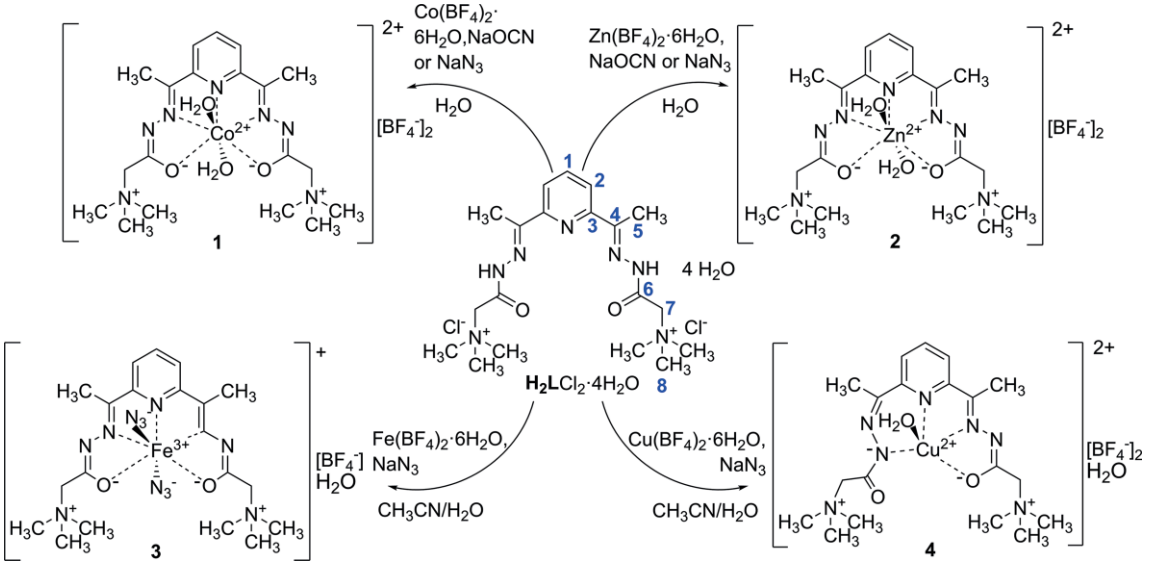

Scheme 1. Synthesis of Co(II) (**1**), Zn(II) (**2**), Fe(III) (**3**), and Cu(II) (**4**) complexes.

lected bond lengths and angles are given in Table 1. The structures of **1**–**4** are displayed in Figure 1.

Table 1. Selected bond lengths [Å] and angles (°) of compounds **1**, **2**, **3**, and **4**.[a]

	1	**2**	**3**	**4**
M–N3	2.176(2)	2.204(2)	2.197(2)	1.943(2)
M–N4	2.186(3)	2.231(3)	2.208(2)	1.986(2)
M–N5			2.190(2)	
M–N6				1.950(2)
M–N8			2.053(3)	
M–N11			2.058(3)	
M–O1	2.1423(18)	2.149(2)	2.091(2)	2.0126(19)
M–O2			2.074(2)	
M–O1w	2.1742(19)	2.173(2)		2.266(2)
O1–M–N3	71.25(7)	71.18(8)	71.80(8)	78.55(9)
O1–M–N4	141.52(5)	140.53(5)	141.67(8)	158.40(8)
O1–M–N5			148.45(8)	
O1–M–N6				109.06(8)
O1–M–O2			76.92(8)	
O1–M–O1w	85.77(8)	86.08(9)		95.31(8)

[a] M = Co (**1**); Zn (**2**); Fe (**3**); Cu (**4**).

In the structures of the complexes **1**–**3**, the pentadentate 2,6-diacetylpyridine dihydrazone ligand (**L**) forms four in-plane fused five-membered chelate rings. Two additional ligands (H_2O in **1** and **2** and N_3^- in **3**) fulfill the distorted pentagonal-bipyramidal coordination spheres. As indicated by the NMR spectra of the Zn(II) complex, the zwitterionic ligand **L** coordinates to the Co(II), Zn(II) and Fe(III) centers in **1**, **2** and **3**, respectively, through the pyridine and two imine nitrogen atoms, as well as two enolate oxygen atoms.

The complexes $[Co\mathbf{L}(H_2O)_2](BF_4)_2$ (**1**) and $[Zn\mathbf{L}(H_2O)_2](BF_4)_2$ (**2**) form isostructural crystals. In the unit cells of **1** and **2**, the complex cations $\{[Co\mathbf{L}(H_2O)_2]^{2+}$ and $[Zn\mathbf{L}(H_2O)_2]^{2+}\}$ and BF_4^- anions lie at the special positions (two-fold axis of symmetry, Wychoff positions 2*e* and 2*f*). Two-fold axis of symmetry passes through the Co1, N4 and C10 atoms in **1** and Zn1, N4 and C10 in **2**, as well as, through the B1 and B2 in **1** and **2** (Figure S2). The in-plane *cis* bond angles in **1**, **2** and **3** cover the ranges 70.78–76.96°, 70.06–79.09° and 69.83–76.92°, and the out-of-plane *trans* bond angles are 176.26°, 178.6° and 174.68°, respectively. Among in plane *cis* bond angles, O–M–N is the closest to the value of 72° expected for an ideal pentagonal-bipyramidal structure [O1–Co1–N3 71.25(7)°, O1–Zn1–N3 70.99(14)°, O1–Fe1–N3 71.80(8)° and O2–Fe1–N5 71.62(8)°], while the largest deviation is observed for the O–M–O open angle [O1–Co1–$O1^a$ 76.96(10)°, O1–Zn1–$O1^b$ 79.09(19)° and O2–Fe1–O1 76.92(8)°, where a and b stand for symmetry operations 1/2 – *x*, *y*, 1/2 – *z* and 1.5 – *x*, *y*, 1/2 – *z*, respectively].

The M–L bond lengths observed in **1**, **2** and **3** are similar to those reported for $[Co\mathbf{H_2L}(NCS)_2]^{2+}$,[35] $[Zn\mathbf{H_2L}(NCS)_2]^{2+}$[36] and $[Fe(\mathbf{L})(NCS)_2]^{+}$[37] complexes with the same 2,6-diacetylpyridine dihydrazone ligand and for the structurally related $[Co(H_2dapsox)(H_2O)(MeOH)]^{2+}$[38] and $[Fe\{H_2dapsox(H_2O)\}]^{2+}$[17] complexes, as well (Table S3). As expected, coordination of the protonated form of the ligand in $[Co\mathbf{H_2L}(NCS)_2]^{2+}$,[35] $[Zn\mathbf{H_2L}(NCS)_2]^{2+}$,[36] $[Co(H_2dapsox)(H_2O)(MeOH)]^{2+}$[38] and $[Fe\{H_2dapsox(H2O)\}]^{2+}$[17] results in somewhat longer $M–O_{amide}$ distances compared to those observed in complexes **1**, **2**, **3** and $[Fe(\mathbf{L})(NCS)_2]^{+}$[37] (Table S3). In the structure of **4**, the ligand behaves as a tetradentate forming in-plane 5–5–6 combination of the chelate rings, with N_{py}, N_{imine},O_{am} and $N_{hydrazide}$ as a set of ligator atoms. The additional H_2O ligand fulfills a distorted square-based pyramidal coordination sphere. A tetradentate coordination of the ligand **L** to Cu(II) could also give in-plane 5–5–5 combination of the chelate rings through a different set of ligator atoms: N_{py}, two N_{imine} and O_{am} (Scheme S1 in the Supplementary material). Structurally related square pyramidal copper(II) complexes $[Cu(dapsox)(H_2O)]\cdot H_2O$[39] and $[Cu(Hdapsox)(H_2O)]ClO_4$,[40] with dioxamohydrazide $H_2dapsox$[2] as a tetradentate ligand, have been described previously by some of us. In general, the ligand $H_2dapsox$ differs from $H_2\mathbf{L}^{2+}$ in the

Full Paper
doi.org/10.1002/ejic.202000415

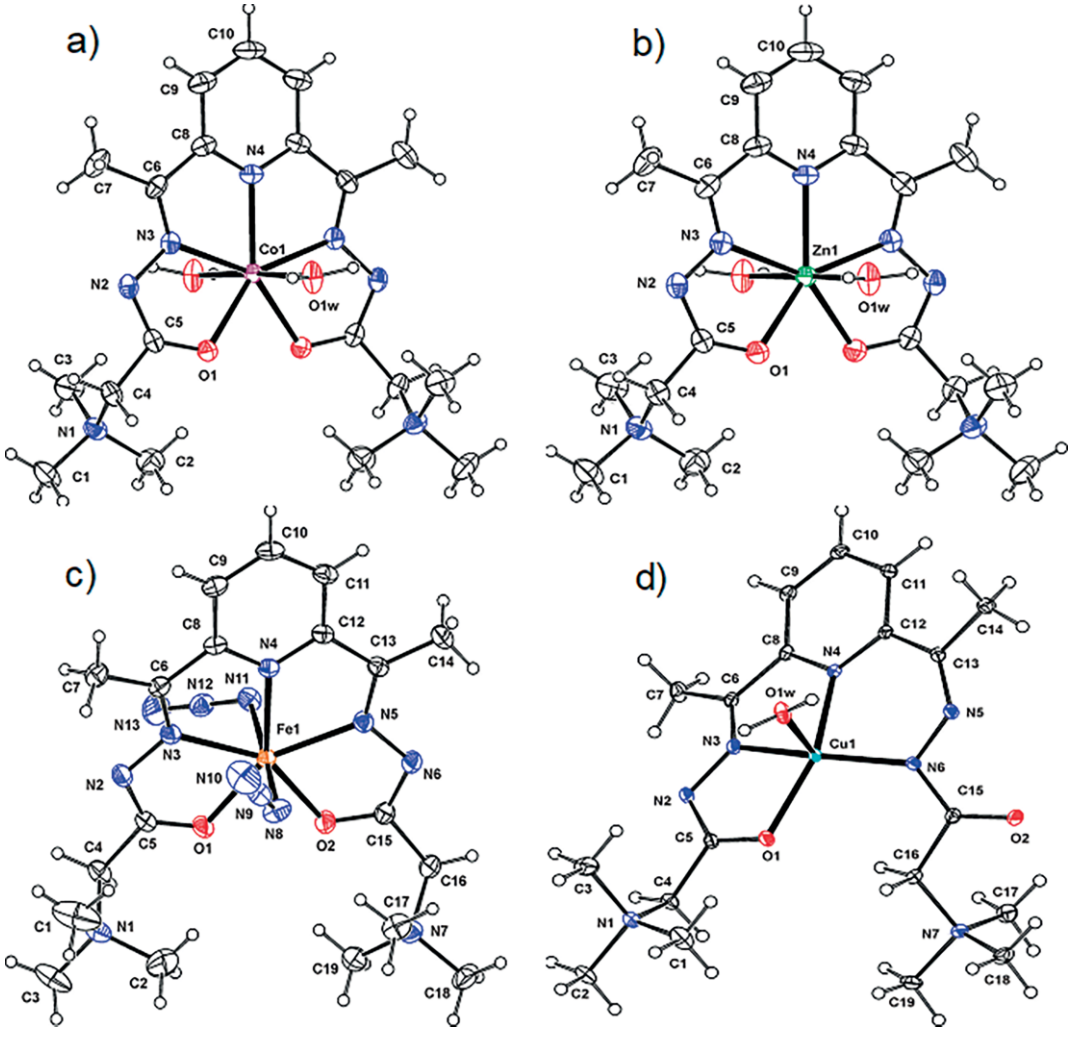

Figure 1. ORTEP plot of **1**(a), **2**(b), **3**(c) and **4** (d) from the X-ray crystal structures with thermal ellipsoids at 30 % probability for non-H atoms and open circles for H-atoms. BF_4^- ions and water molecule are omitted for clarity.

number of potential donor atoms (11 vs. 7), although in both cases some of them are mutually exclusive. The H_2dapsox is able to form different in-plane combinations of the five- and six-membered chelation rings upon coordination to metal ions either as pentadentate or tetradentate ligand,[2,38–40] while a pentadentate coordination of $H_2\mathbf{L}^{2+}$ or **L** to metal ion can only be achieved by formation of four fused five-membered chelation rings. Therefore, the geometrical isomerism of metal complexes with H_2dapsox or its deprotonated forms is much more intricate compared to that of metal complexes with $H_2\mathbf{L}^{2+}$ or **L**. Upon the tetradentate coordination of dapsox^{2-} or Hdapsox$^-$ to copper(II) ion three fused metal-chelate rings are formed: a central six-membered ring (Cu–N-C-C-N-N) with five-membered rings (Cu–O–C–C–N and Cu–N–C–C–N) at each side of it (the asymmetric 5–6–5 combination of the chelate rings).[39,40] In all three complexes [Cu**L**(H_2O)](BF_4)$_2$·H_2O (**4**), [Cu(dapsox)(H_2O)]·H_2O[39] and [Cu(Hdapsox)(H_2O)]ClO_4,[40] the corresponding ligands are asymmetrically coordinated to metal ions. The in-plane combination of the chelate rings 5–6–5 is not possible for [Cu**L**(H_2O)](BF_4)$_2$·H_2O (**4**) complex. The average bond length between the Cu(II) center and the tetradentate ligand is longer in **4** (ca. 1.973 Å) than in the case of [Cu(dapsox)(H_2O)]·H_2O (ca. 1.961 Å) and [Cu(Hdapsox)(H_2O)]ClO_4 (ca. 1.959 Å). This might be a consequence of the presence of two positively charged quaternary ammonium residues in the structure of **L** and suggests a somewhat less electron density on the Cu(II) center in **4** in comparison to the Cu(II) centers in complexes with H_2dapsox. As a consequence of such electronic properties the apical Cu–aqua [Cu1–O1w = 2.266(2) Å] bond is shorter in **4** than the corresponding ones in [Cu(dapsox)(H_2O)]·H_2O and [Cu(Hdapsox)(H_2O)]ClO_4 complexes, and the Cu(II) ion is displaced by 0.2112(3) Å from the mean coordination plane towards the apical water oxygen. The in-plane *trans* bond angles are very bent and are almost identical [N3–Cu1–N6 159.52(16)° and N4–Cu1–O1 158.32(15)]. The angular structural parameter (τ) is used to describe the degree of trigonality, within the structural continuum between trigonal bipyramidal and square-based pyramidal geometry [$\tau = (\beta - \alpha)/60$, where β and α are the two largest angles around the central atom; τ is 0 for regular square based pyramidal geometry and 1 for regular trigonal bipyramidal geometry].[41] The [Cu(dapsox)(H_2O)]·H_2O and [Cu(Hdapsox)(H_2O)]ClO_4 show a greater degree of trigonal dis-

Full Paper
doi.org/10.1002/ejic.202000415

tortion from square pyramidal configuration compared to complex **4**, as indicated by τ values of 0.11 and 0.08 vs. 0.01, respectively (cf. Table S4; comparison of the puckering parameters of the chelate rings is given in Table S5).

The bond lengths within the ligand fragments >C–N–N–C–O are affected by the asymmetric coordination of **L** to Cu(II) in **4**. The C15–O2 and C5–O1 bond lengths of 1.240(3) Å and 1.277(3) Å, respectively, are in accordance with a higher single bond character of the latter with O1 being coordinated to Cu(II). In addition, the N6–C15 and N2–C5 bond lengths of 1.351(3) Å and 1.325(4) Å, respectively, are in agreement with a higher double bond character in the latter. Both hydrazine fragments, N2–N3 [1.373(3) Å] in the five-membered chelation ring and N5–N6 [1.392(3) Å] in the six-membered chelation ring are shorter than normal single bonds and longer than normal double bonds, which is a clear indication of the π electron delocalization due to double deprotonation of **L**. Interestingly, the Cu–O bond length in complex **4** of 2.013(2) Å is slightly longer than those observed in [Cu(dapsox)(H_2O)]·H_2O[39] and [Cu(Hdapsox)(H_2O)]ClO_4[40] complexes [1.993(2) and 1.991(3) Å, respectively]. The opposite is expected based on the single C–O bond character in **4** and the double C–O bond character in the latter two complexes. This might be explained by the fact that the Cu(II)–**L** bond lengths in **4** are additionally affected by the bond angle strain in the five-membered rings and torsional strain in the six-membered ring (see SI).

Description of the double-layer crystal structures of **1**–**4** and intermolecular interactions within them is given in SI (Figures S2–S4 and Tables S6–S11).

X-Band EPR Measurements

Paramagnetic complexes **1**, **3**, and **4** were studied by X-band EPR spectroscopy in frozen solution and in solid state.

The X-band EPR spectrum of **1** in frozen DMF (Figure 2) shows a rhombic signal with *g*-values at 4.84, 4.26, and 1.99, which is consistent with a divalent cobalt ion in the high spin state (S = 3/2). Additionally, a hyperfine coupling pattern with eight lines is resolved on the *g*-value at 1.99, originating from coupling of the electron spin with the nuclear spin I of a single ^{59}Co nucleus (I = 7/2, 100 %).

The spectrum of **4**, also recorded in frozen DMF solution, (Figure 3) displays a slightly rhombic signal as well, with *g*-values centered at 2.21, 2.06, and 2.03, which is consistent with a complex containing a Cu(II), d^9, ion in the ligand environment of a bishydrazone chelate. The characteristic hyperfine coupling pattern to the central copper nuclei ([63/65] Cu, I = 3/2, 100 % total natural abundance) on g = 2.21 with a hyperfine coupling constant, A, of 15.02 mT is well-resolved. Additionally, a seven-line super-hyperfine splitting pattern on g = 2.06 is observed and partly resolved. This agrees well with the chelate's coordination mode, as observed in the solid-state molecular structure obtained from sc-XRD, where three nitrogen atoms are bound to the Cu center. Thus, a reasonable simulation of the experimental spectrum was obtained with additional super-hyperfine coupling between copper center's unpaired electron with the nuclear spin of three equivalent nitrogen atoms (^{14}N, I = 1, 99.6 %) was considered.

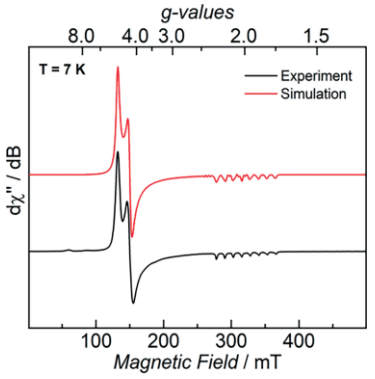

Figure 2. CW X-band EPR spectrum of **1** at 7 K, recorded in 5 mM frozen solution in DMF (black trace), and its simulation (red trace). Experimental conditions: microwave frequency ν = 8.956 GHz, modulation width = 0.1 mT, microwave power = 0.1 mW, modulation frequency = 100 kHz, time constant = 0.1 s. The simulation was performed with effective *g*-values of: g_1 = 4.84, g_2 = 4.26, g_3 = 1.99, with W_1 = 3.80 mT, W_2 = 3.70 mT and W_3 = 4.00 mT, and hyperfine coupling to one ^{59}Co (I = 7/2, 100 %) nucleus with A_3 = 12.38 mT (344.76 MHz).

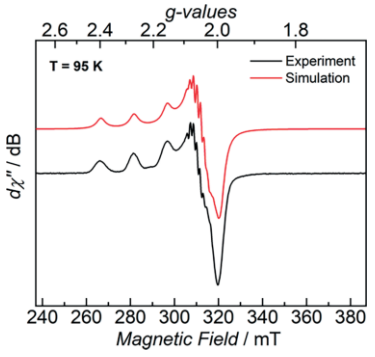

Figure 3. CW X-band EPR spectrum of **4** at 95 K, recorded in 1 mM frozen solution in DMF (black trace), and its simulation (red trace). Experimental conditions: microwave frequency ν = 8.944 GHz, modulation width = 0.3 mT, microwave power = 1.0 mW, modulation frequency = 100 kHz, time constant = 0.1 s. The simulation was performed with effective *g*-values of: g_1 = 2.21, g_2 = 2.06, g_3 = 2.03, with W_1 = 2.80 mT, W_2 = 0.46 mT and W_3 = 3.00 mT, hyperfine coupling to one ^{63}Cu/^{65}Cu (I = 3/2, 69.15 %/30.85 %) nucleus with $A_{Cu,1}$ = 15.02 mT (464.68 MHz), and super-hyperfine coupling to three equivalent ^{14}N nuclei (I = 1, 99.64 %) with $A_{N,2}$ = 1.62 mT (46.77 MHz).

The X-band EPR spectrum of the Fe complex **3** shows a rhombic signal at 7 and 92 K, but the simulation of the experimental data was not possible, because the assignment of the *g*-values was not straightforward (measurements at different concentrations and temperatures did not result in a better resolution of the spectrum. Preliminary spectra are given in Figure S6). The CW X-band EPR spectra of **1**, **3**, and **4** in frozen solution are in accordance with the solid state measurements (see Figure S5 and S6 in the supporting information), which supports the preservation of the structure in solution.

Cyclic Voltammetry

Formal redox potentials of the Fe(III) **3**, Co(II) **1** and Cu(II) **4** complexes were estimated in MOPS buffer solution (pH = 7.4,

Full Paper
doi.org/10.1002/ejic.202000415

c = 60 mM, *I* = 150 mM) and in DMF (Table 2 and Figure 4). For all measurements an Ag/AgCl wire was used as pseudo reference electrode, therefore an internal reference system (Fc/Fc^+) was introduced and its potential found at +0.53 V vs. Ag/AgCl {$E^0(Fc/Fc^+)$ = 0.40 V vs. SHE}. The cyclic voltammogram in the potential range between −1.3 V and +1.3 V in DMF demonstrates one reversible half-wave potential in the case of Fe(III) and Co(II) complexes at −0.23 V and −0.81 V vs. Ag/AgCl electrode, respectively. By way of comparison, structurally related $[Fe(dapsox)(H_2O)_2]ClO_4$ exhibits a reversible couple at −0.13 V vs. Ag/AgCl electrode in DMSO.[17] More negative redox potential for **3** suggest that the Fe(II) form of this complex is somewhat less stabilized, which may be related to the presence of N_3^- anions in the coordination sphere of the Fe center in DMF solutions. In aqueous solution a reversible redox process is observed at −0.17 V vs. Ag/AgCl, which is close to that of $[Fe(dapsox)(H_2O)_2]ClO_4$,[17] suggesting that at pH 7.4 both Fe(III) complexes exist in the aqua-hydroxo form. The redox potential observed for **1** in DMF corresponds to the Co(II)/Co(I) redox couple and is similar to that observed for a Schiff base Co(II) complexes, containing a crown-like cavity with Ca^{2+} in a close proximity.[42] It seems that an effect of two cationic quaternary ammonium residues on the reduction of Co(II) is similar to that of Ca^{2+}. By way of comparison the redox potential of the Schiff base Co(II) complex from the literature with nearby Ca^{2+} is for 0.3 V more positive than that of the complex without any additional cation, whereas presence of other cations such as Ba^{2+}, Sr^{2+}, Na^+ and K^+ exhibits significantly smaller effects. Oxidation of Co(II) was not observed in DMF. However, in aqueous solution a Co(II) to Co(III) quasi-reversible transformation appears at −0.17 V vs. Ag/AgCl (Figure S7), as in the case of **3**. This suggests that formation of Co(III) is more feasible at pH 7.4 in a buffer solution than in DMF, where it is coupled to a deprotonation of an aqua ligand and stabilization of Co(III) in the aqua-hydroxo form. Since d^6 configuration of Co(III) does not support stable PBP geometries,[2,3] oxidation of **1** requires a certain structural rearrangement and therefore the observed redox process is of lower intensity and less reversible than that in the case of **3**. The redox behavior of the Cu(II) complex is more complex. The reduction that is observed at −0.19 V in DMF is probably followed by disproportionation of Cu(I) and deposition of a copper species onto the electrode surface, which then undergoes oxidative dissolution back into DMF solution.

Table 2. Redox potentials (half-wave potentials, $E_{1/2}$, anodic, E_{pa}, or cathodic, E_{pc}, peak potentials) vs. Ag/AgCl reference electrode of Fe(III), Co(II) and Cu(II) complexes in DMF and MOPS buffer solutions (pH = 7.4, c = 60 mM, I = 150 mM, complex concentration 1 mM).

	E [V] vs. Ag/AgCl in DMF	*E* [V] vs. Ag/AgCl in buffer
Fe (III)	−0.23 V ($E_{1/2}$)	−0.17 V ($E_{1/2}$)
Co (II)	−0.81 V ($E_{1/2}$)	−0.17 V ($E_{1/2}$)
Cu (II)	−0.19 V ($E_{1/2}$)	−0.22 V (E^1_{pa})
	0.67 V (E_{pa})	−0.02 V (E^2_{pa})
	0.62 V (E_{pc})	+0.13 V (E^3_{pa})
		−0.05 V (E^1_{pc})
		−0.23 V (E^2_{pc})
		−0.44 V (E^3_{pc})

The related stripping process is observed at +0.67 V (E_{pa}) (Figure S8). In aqueous solutions more processes can be observed (Table 2, Figure S9) due to the less stable Cu(I) species and more favorable disproportionation and deposition processes.

Analysis of these processes is out of the scope of the present work. However, we can assume that three cathodic peaks are related to Cu(II) to Cu(I) (E^1_{pa}/E^3_{pc}), Cu(II) to Cu(0) (E^2_{pa}/E^2_{pc}) and Cu(I) to Cu(0) (E^3_{pa}/E^1_{pc}) reductions, respectively. The three anodic processes probably correspond to the oxidative generation of different copper species by stripping processes.[43]

The Zn complex was electrochemically silent, confirming also that the ligand is redox inactive and that all observed redox processes of **1**, **3** and **4** are metal-centered.

Reactivity with Superoxide

Redox active **1**, **3** and **4** complexes were investigated in our stopped-flow assay to directly evaluate their capabilities to catalytically degrade the superoxide radical anion. Only the copper complex **4** was capable to facilitate efficient catalytic removal of $O_2^{\bullet-}$ in aqueous buffered systems. The highest rate was deter-

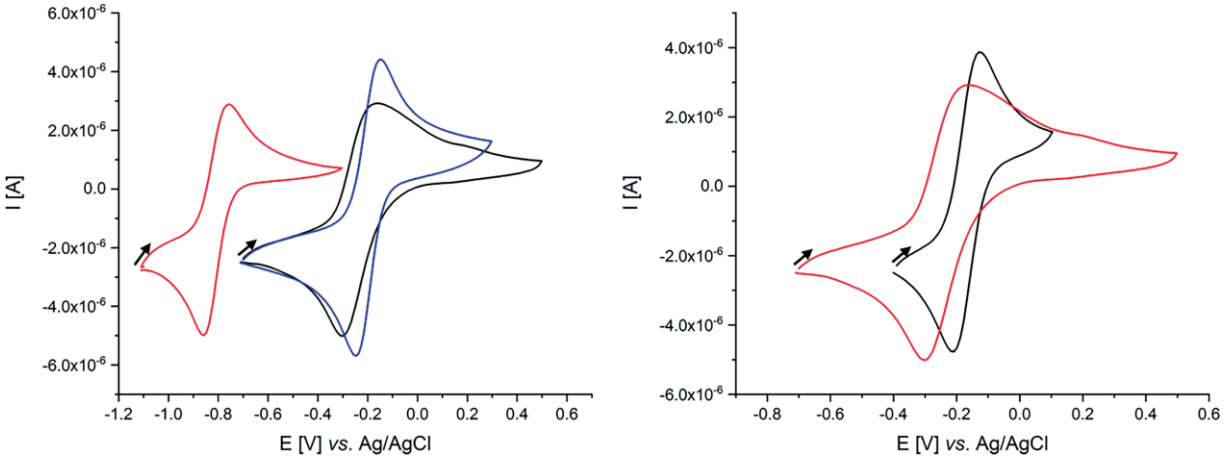

Figure 4. Left: Cyclic voltammograms of the Fe(III) complex (black), Co(II) complex (red) and copper complex (blue) in DMF solution. Right: Comparison of the cyclic voltammograms of the Fe(III) complex in DMF (red) and in buffer solution (black). Scan rates 0.1 V/s.

mined in MOPS buffered solution at pH = 7.4, while the rate diminished in presence of phosphate as usually expected due to the competition between superoxide and phosphate for the binding to the metal center (Figure 5).[44] SOD activity of **1** was not expected, despite the observed redox potential (–0.17 V vs. Ag/AgCl that corresponds to ca. 0 V vs. SHE) that still fits in the potential window for superoxide reduction and oxidation. This is because the PBP coordination environment does not provide suitable reversibility of the Co(II)/Co(III) couple required for the fast redox cycling within SOD catalysis. Furthermore, the fact that also the iron complex **3**, with the same redox potential as that reported for the analogues [Fe(dapsox)$(H_2O)_2$]ClO_4 complex that is a known SOD mimetic,[17] does not demonstrate SOD activity, supports our postulations that suitable redox potentials alone are not a guarantee for the complex to be capable of catalytic superoxide removal.[45–47] One of the reasons is usually the operation of an inner-sphere SOD mechanism in the case of complexes with a labile or vacant coordination site, whereas the electrochemically measured redox potentials are more of significance for outer-sphere electron transfer processes. The coordination changes the electronic situation of both the metal complexes and superoxide, thus effecting the possible dismutation, making it either favorable or not. Another reason is related to the stability of metal-(hydro)peroxo species as an intermediate product of an inner-sphere superoxide reduction. Efficient release of hydrogen peroxide from the metal center is crucial for the catalysis and therefore high stability of metal-(hydro)peroxo species or its less favorable protonation may suppress the SOD activity by product inhibition.[48–50] This might be the reason for the lack of the catalytic activity of **3**, where positively charge residues could contribute to increased stabilization of the putative Fe(III)-peroxo and/or slow down its deprotonation. We have previously shown that increase of a positive charge on the porphyrin ring does not necessary influences corresponding redox potential of the Fe center, but it strongly influences its kinetic behavior.[51]

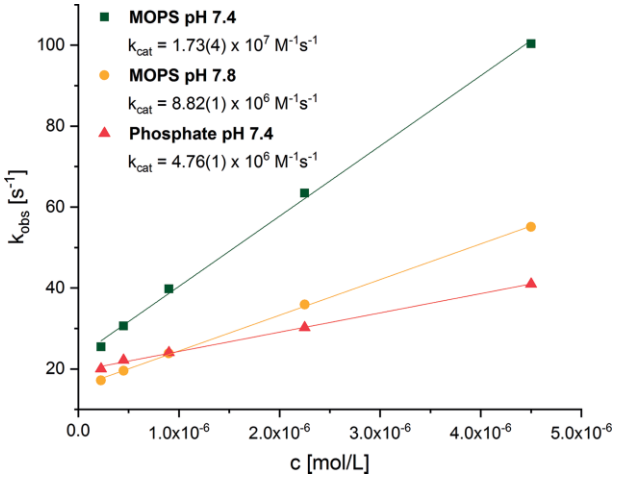

Figure 5. Determination of second order rate constants (k_{cat}) for catalytic superoxide removal, in various buffered systems, for the Cu(II) complex **4**.

On the other hand, a quite significant SOD activity of **4** with k_{cat} = 1.73 × 10^7 M^{-1} s^{-1} might be related to a higher kinetic lability of both Cu(II) and Cu(I), with the d^9 and d^{10} electron configurations, respectively, in comparison to that of the Fe(III) and Fe(II) centers. Also, the corresponding Cu(II)-peroxo is expected to be thermodynamically less stable than Fe(III)-peroxo, due to the lower positive charge of the metal center. Because it is known that the free Cu(II)-aqua species possesses a significant SOD activity that exceeds that of the natural enzyme,[52,53] the observed activity of the complex could, at least in part, result from the complex dissociation and release of free Cu(II). The ultra-high resolution ESI-MS measurements (Figure S11–S14) did not indicate even traces of the free ligand, suggesting that the Cu(II) complex is intact in solution.

Since Cu(I) obtained upon reaction with superoxide, within the catalytic cycle, might undergo disproportionation and complex dissociation, we performed the CV measurements where superoxide is generated in situ by electrochemical reduction of oxygen (see Experimental Section) in the presence of **4** (Figure 6). Importantly, the sharp peak at 0.42 V that is related to the oxidation of the Cu species deposited on the electrode surface, as a consequence of complex dissociation/disproportionation, disappears in the presence of oxygen. Even when the cycling is repeated or run in another direction, the signal does not appear. This clearly suggests that the Cu(I) form of the complex is protected from decomposition in the presence of oxygen species upon reacting with them. Thus, there is no indication of free Cu species formation under catalytically related conditions, i.e. in the presence of superoxide, suggesting that the measured catalytic rate constant results from the SOD activity of the intact complex.

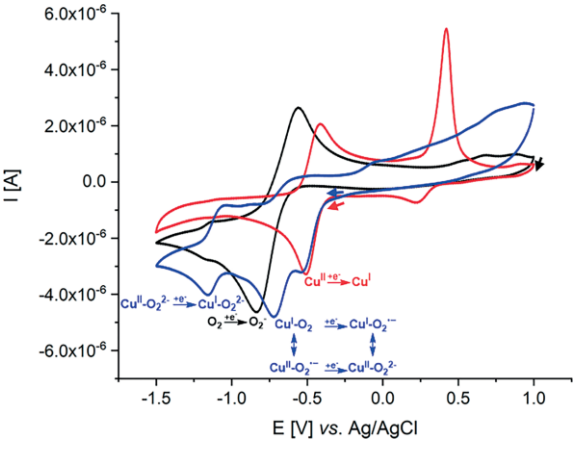

Figure 6. Cyclic voltammograms of DMSO solution saturated with pure oxygen ([O_2] = 2.1 mM; black), Cu(II) complex **4** (1 mM) in DMSO solution purged with nitrogen (red) or pure oxygen (blue).

Furthermore, in the presence of **4**, re-oxidation of the in situ formed superoxide (anodic peak at –0.56 V) was not observed due to its consumption upon reacting with the Cu species. Interestingly, oxygen atmosphere does not affect the reduction of Cu(II) to Cu(I), but two new cathodic peaks appear. The one that appears at –0.72 V is related to the reduction of oxygen bound to Cu(I) (which is anodically shifted in comparison to the reduction of free oxygen), resulting in Cu(I)-superoxo/Cu(II)-peroxo. This species is also a possible intermediate within SOD catalytic cycle. The second peak could be assigned to the further reduction and generation of a putative Cu(I)-peroxo. Posi-

Full Paper
doi.org/10.1002/ejic.202000415

tively charged residues on the ligand might have a stabilizing effect on a Cu(I)-superoxo/Cu(II)-peroxo species enabling observation of its further quasi-reversible reduction. More detailed characterization of these processes is out of the scope of the present works, but will be considered in future studies.

A similar electrochemical experiment we have performed with the Fe complex, **3**, in order to get an information on a possible stoichiometric interaction between the reduced Fe(II) form of the complex and electrochemically generated superoxide.

In DMSO we could clearly observe that in the presence of **3**, superoxide is decomposed/transformed prior to its possible re-oxidation, demonstrated by absence of the superoxide cathodic signal (Figure 7). Such observation suggests that **3** in the Fe(II) form is capable to stoichiometrically react with superoxide in DMSO, probably due to dissociation of one or two N_3^- anions, which increases overall complex charge and provides labile coordination site for the superoxide binding. This postulation is supported by the presence of two cathodic and two anodic processes of **3** in DMSO, related to the equilibrium between the species with dissociated and coordinated azide ligands (Scheme in Figure 7). The anodically shifted signal is related to the redox couple with coordinated azide anions and lower overall charge. The relatively lower intensity of the E^1_{pc} signal compared to E^2_{pc} indicates that in the Fe(III) form, the equilibrium is shifted more into direction of the di-azide form. These electrochemical observations again demonstrate the importance of electrostatic interactions when it comes to anion binding, in general, and superoxide binding, in particular.

In DMF, where an oxygen saturated solution of higher concentration could be obtained ($[O_2]$ = 4.8 mM), we performed the experiment with varied amounts of the Fe complex. A shift of the reduction peak of superoxide was observed (Figure S10), which is also in agreement with the coordination of superoxide to the iron center, as reported in the literature.[54]

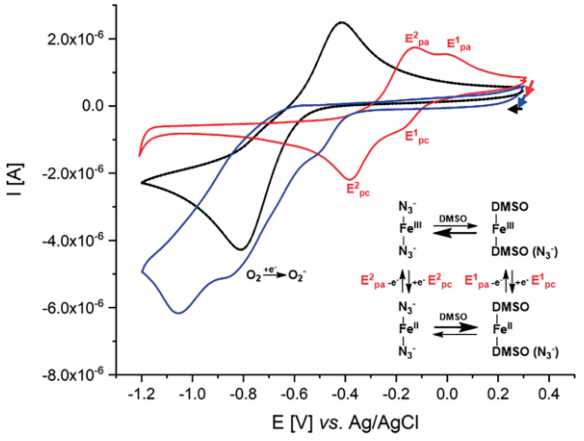

Figure 7. Cyclic voltammograms of DMSO solution purged with pure oxygen (black), Fe(III) complex **3** in DMSO solution purged with nitrogen (red) or oxygen (blue).

Conclusion

Besides standard physico-chemical and structural characterization of the Co(II), Zn(II), Fe(III) and Cu(II) complexes of the 2,6-diacetylpyridine dihydrazone type ligand, we have also investigated their redox behavior and tested their potential SOD activity. Knowing that the structurally related Fe(III) complex [Fe(dapsox)$(H_2O)_2$]ClO_4, which was previously studied by some of us, possesses the SOD activity,[17] we wanted to probe whether the presence of two positively charged quaternary ammonium residues on the zwitterionic ligand **L** induce an effect on a potential SOD activity and general redox behavior. A few conclusions could be drawn based on the obtained results and observed reactivity mode towards superoxide (summarized in Scheme 2).

Since no difference in the redox potential for the Fe(III)/Fe(II) couple in a buffer solution was observed between that for **3**

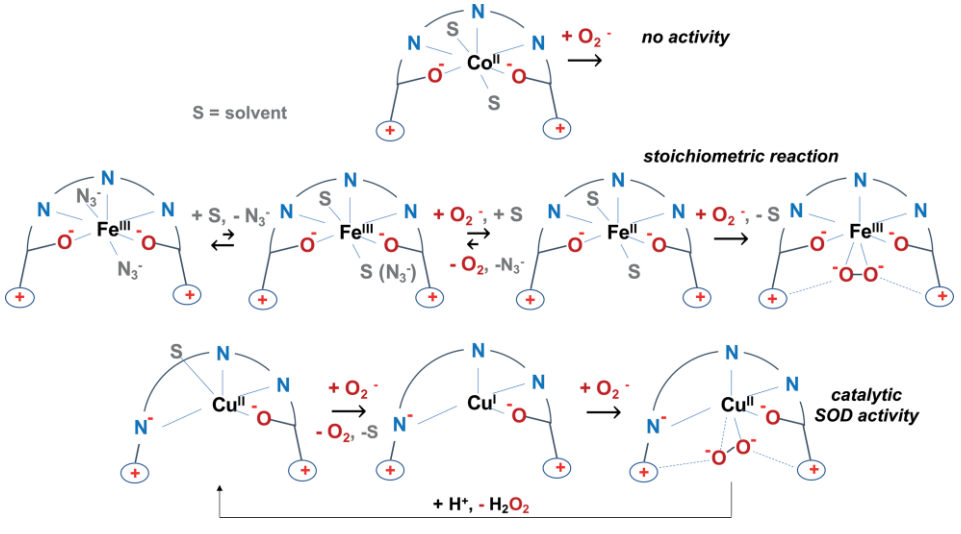

Scheme 2. Summary of observed reactivity toward superoxide for **1**, **3** and **4**.

Full Paper
doi.org/10.1002/ejic.202000415

and [Fe(dapsox)$(H_2O)_2$]ClO_4, it is clear that quaternary ammonium cations in **L** do not affect redox properties of the Fe center. This can be explained by the fact that there is no electronic communication between these positive residues and the metal center, because they are not conjugated and spatial distribution of charged groups in the PBP coordination sphere around Fe(III) or Fe(II), respectively, seems not to support required interactions. The same behavior we have observed in the case of highly positively charged Fe and Mn porphyrins.[51] Although the redox potential remains unchanged, different from [Fe(dapsox)$(H_2O)_2$]ClO_4 the complex **3** does not exhibit SOD activity, demonstrating that the formal redox potential is not the only criteria for a metal complex to be an SOD mimetic. For example, the nature/reactivity of a potential Fe(III)-peroxo intermediate species can also be crucial for the overall catalysis. In that line, we can speculate that two positively charged aprotic groups nearby the coordinated O_2^{2-} anion of a putative Fe(III)-peroxo species contribute to its stabilization and hinder its efficient protonation and release of H_2O_2. Such stabilization of Fe(III)-peroxo by nearby Ca^{2+} within covalently bound crown-ether functionality we have previously observed in the case of a porphyrin complex, which has resulted in a lack of SOD activity and operation of stoichiometric reaction between Fe(II) form of the porphyrin complex and superoxide.[55] The redox potential that corresponds to the Co(III)/Co(II) couple of **1** in a buffer solution is identical to that of **3** and [Fe(dapsox)$(H_2O)_2$]ClO_4, respectively. The complex **1** is also SOD inactive, which is probably related to kinetically unfavorable oxidation of the Co(II) species in the PBP coordination geometry.[2,3] In general, the SOD catalysis based on Co(II)/Co(III) cycling is not expected due to kinetically inert nature of Co(III). On the other hand kinetic lability of both Cu(II) and Cu(I) species as well as a tetradentate coordination of the ligand **L** that does not require significant reorganization upon Cu(II)/Cu(I) redox cycling of the complex **4**, together with an appropriate redox potential, are optimal preconditions for a complex to be SOD active. Indeed, the observed catalytic rate constant (1.73×10^7 M^{-1} s^{-1}) for the superoxide dismutation by **4** is quite high and is comparable to that of the copper complexes with amino acids, which was determined by a pulse radiolysis method.[53] We would like to point out that the superoxide dismutation by copper complexes is predominantly studied in the literature by indirect assays, where IC_{50} values rather than second order catalytic rate constants k_{cat} (obtained by direct stopped-flow or pulse radiolysis methods) are reported.[56] On one hand it is known that indirect assays may result in putative activity values that are influenced by side reactions,[17,44] and on the other hand IC_{50} and k_{cat} values cannot always be directly compared. Thus, as another comparison we can mention k_{cat} values of Cu(II) complexes of naturally occurring disulfides, as oxidized glutathione, cystine, homocystine or α-lipoic acid that are close to 10^6 M^{-1} s^{-1}.[57] It seems that there is a need for a further characterization of copper based SOD mimetics by direct methods. The postulated mechanistic aspects of the redox reactivity and SOD activity of the studied complexes and their modulation by surrounding positive charge will also be further investigated.

Experimental Section

Materials and Methods

2,6-Diacetylpyridine (99 %) and Girard's T reagent (99 %) were obtained from Aldrich. IR spectra were recorded on a Nicolet 6700 FT-IR spectrometer using the ATR technique in the region 4000–400 cm^{-1} (s strong, m medium, w weak). ^1H and ^{13}C NMR spectra were recorded on Bruker Avance 500 spectrometer (^1H at 500 MHz; ^{13}C at 125 MHz) at room temperature using TMS as internal standard in D_2O for ligand and in [D_6]DMSO for Zn(II) complex. Chemical shifts are expressed in ppm (δ) values and coupling constants (J) in Hz.

Cyclic voltammetry experiments were performed on a Metrohm PGSTAT 101 potentiostat, controlling by Nova 1.6 software. A conventional three electrode-arrangement (Deutsche Metrohm GmbH & Co. KG) was employed consisting of a gold disc working electrode (geometric area 0.07 cm^2), a platinum rod as counter electrode and either an Ag/AgCl (3 M NaCl) reference electrode for aqueous solution or an Ag wire for measurements in organic solvents. MOPS (3-morpholinopropane-1-sulfonic acid) buffer solution (pH = 7.4, c = 60 mM, I = 150 mM), DMF or DMSO were used as solvents. Contained NaCl in the buffer solution was conducted as supporting electrolyte. For measurements in organic solvents tetrabutylammonium tetrafluoroborate (0.1 M) was added as conducting salt and ferrocene as internal reference standard. All measurements were performed with the 0.1 V/s scan rate under nitrogen atmosphere and at 21 °C. For comparison reasons, measurements in different solvents were referenced to Ag/AgCl (Fc/Fc^+ vs. Ag/AgCl +0.53 V in DMF).[58] To perform CVs in the presence of oxygen, an oxygen saturated solution was used obtained by purging dry oxygen into solution for 1 min/mL ([O_2] = 2.1 mM in DMSO; [O_2] = 4.8 mM in DMF).[59,60]

Stopped-flow measurements were performed on a Biologic SFM-400 four syringe stopped-flow system using only the first three syringes and a Berger Ball mixer to minimize mixing effects between aqueous buffered solutions and DMSO solutions of KO_2. A J&M TIDAS S MMS UV/Vis diode array detector (integration time 0.5 ms, 180 nm – 720 nm wavelength) and an Energetiq LDLS ENQ EQ-99-FC laser driven light source were used. The ratio between buffer and DMSO solution was kept constant at 9:1. Superoxide solutions were prepared by suspending 220 – 240 mg of KO_2 in 20 mL of dry DMSO. The suspension was stirred for at least 30 min under inert atmosphere before the suspension was filtered through a PTFE syringe filter (Ø = 0.45 μm) to give a saturated KO_2 solution, which was transferred to the stopped flow setup. The buffers were prepared from commercially available 4-Morpholinepropanesulfonic acid and Sodium dihydrogen phosphate salts. Buffer concentration was 60 mM and ionic strength was set to 150 mM for each buffer by addition of NaCl. Millipore water was used for all buffer solutions and all buffers were treated with Chelex® 100 chelating resin for at least 24 h before use. A stock solution (1.00×10^{-4} M) of complex was prepared in each buffer (10 % DMSO content), which was diluted in the respective buffer to give a series of concentrations suitable for the stopped flow experiments. Kinetic measurements were performed applying a large excess of superoxide over putative SOD mimetic ([$O_2^{\cdot-}$] = 100 – 200 μM and [SODm] = 0.25 – 4.5 μM). All kinetic data were fitted with the program Biokine 32 V4.80. Each k_{obs} value represents an average of at least nine measurements. k_{cat} was determined from the slope of k_{obs} vs. [SODm]. All measurements were performed at 21 °C.

EPR spectra were recorded on a JEOL continuous wave spectrometer JES-FA200, equipped with an X-band Gunn diode oscillator

Full Paper
doi.org/10.1002/ejic.202000415

bridge, a cylindrical mode cavity, and a liquid Helium cryostat. The samples were freshly dissolved in dry DMF under ambient conditions. The solution, sealed in a J. Young EPR tube, was immediately frozen in liquid nitrogen until measured. Solid state samples were grounded before being transferred into EPR tubes at ambient conditions. Analysis and simulation of the data was performed using the software "eview" and "esim", written by E. Bill (E-mail: ebill@gwdg.***de***, MPI for Chemical Energy Conversion, Mülheim an der Ruhr).

Electrospray-ionization MS (ESI-MS) measurements were performed on a UHR-TOF Bruker Daltonik (Bremen, Germany) maXis plus, an ESI-quadrupole time-of-flight (qToF) mass spectrometer capable of resolution of at least 60.000 FWHM. Detection was in positive ion mode, the source voltage was 3.2 kV. The flow rates were 180 µL/hour. The drying gas (N_2), to aid solvent removal, was held at 180 °C and the spray gas was held at 20 °C. The mass spectrometer was calibrated prior to every experiment via direct infusion of Agilent ESI-TOF low concentration tuning mixture, which provided an *m/z* range of singly charged peaks up to 2700 Da in both ion modes.

IR spectroscopy experiments were conducted on a Fourier-Transform Infrared Spectrometer Shimazdu IR Prestige 21.

UV/Vis spectra in DMF and aqueous buffer solutions (Figure S15 and S16) were recorded on an Analytik Jena Specord S600 diode array spectrophotometer.

Synthesis of Ligand ($H_2LCl_2{\cdot}4H_2O$): The synthesis of ligand $\mathbf{H_2L}Cl_2{\cdot}4H_2O$ was described previously.[34] IR: $\tilde{\nu}$ = 3394 (s), 3115 (m), 3071 (m), 3020 (m), 2969 (w), 2934 (w), 1709 (s), 1630 (w), 1568 (w), 1489 (m), 1423 (m), 1366 (w), 1329 (w), 1281 (m), 1228 (m), 1153 (w), 1123 (w), 993 (w), 949 (w), 922 (w), 855 (w), 827 (w), 744 (w), 702 (w), 663 (w) cm^{-1}; elemental analysis calcd. (%) for $C_{19}H_{41}N_7O_6Cl_2$: C 42.70, H 7.73, N 18.34; found C 42.73, H 7.69, N 18.35.

Synthesis of Co(II) Complex (1): The ligand $\mathbf{H_2L}Cl_2{\cdot}4H_2O$ (0.26 g, 0.5 mmol) was dissolved in water (30 mL) and solid $Co(BF_4)_2{\cdot}6H_2O$ (0.17 g, 0.5 mmol) was added. After complete dissolution of $Co(BF_4)_2{\cdot}6H_2O$ in the reaction mixture NaOCN (0.13 g, 2.0 mmol) or NaN_3 (0.13 g, 2.00 mmol) was added. The reaction solution was heated to reflux and stirred for 2 h. After slow evaporation of solvent in a refrigerator (≈ 4 °C) for one week, orange crystals were obtained. Yield 0.11 g (34 %). IR: $\tilde{\nu}$ = 3573 (s), 3052 (m), 1649 (w), 1570 (s), 1488 (m), 1441 (w), 1399 (m), 1370 (w), 1327 (w), 1307 (w), 1262 (w), 1199 (w), 1151 (w), 1051 (s), 972 (w), 910 (w), 811 (w), 748 (w), 675 (w), 597 (w), 522 (w) cm^{-1}; MS (ESI): *m/z* calcd. for $C_{19}H_{31}N_7O_2CoBF_4$: 535.1895, found 535.1898; elemental analysis calcd. (%) for $C_{19}H_{35}B_2CoF_8N_7O_4$: C 34.68, H 5.36, N 14.90; found C 34.73, H 5.41, N 14.85.

Synthesis of Zn(II) Complex (2): The ligand $\mathbf{H_2L}Cl_2{\cdot}4H_2O$ (0.26 g, 0.5 mmol) was dissolved in water (30 mL) and then solid $Zn(BF_4)_2{\cdot}6H_2O$ (0.17 g, 0.5 mmol) was added. After complete dissolution of $Zn(BF_4)_2{\cdot}6H_2O$ in the reaction mixture solid NaOCN (0.13 g, 2.00 mmol) or NaN_3 (0.13 g, 2.00 mmol) was added. The reaction solution was heated to reflux and stirred for 2 h. Yellow needle-shaped crystals suitable for X-ray analysis arose from the reaction solution after two weeks. Yield 0.10 g (31 %). IR: $\tilde{\nu}$ = 3566 (m), 3054 (w), 2977 (w), 1647 (w), 1614 (w), 1572 (s), 1534 (w), 1488 (m), 1442 (w), 1416 (w), 1398 (w), 1370 (w), 1338 (w), 1325 (w), 1303 (w), 1261 (w), 1199 (w), 1155 (w), 1053 (s), 973 (w), 910 (w), 812 (w), 751 (w), 677 (w), 521 (w) cm^{-1}; MS (ESI): *m/z* calcd. for $C_{19}H_{31}N_7O_2ZnBF_4$: 540.1854, found 540.1858; elemental analysis calcd. (%) for $C_{19}H_{35}B_2ZnF_8N_7O_4$: C 34.34, H 5.31, N 14.75; found C 34.29, H 5.37, N 14.82.

Synthesis of Fe(III) Complex (3): The ligand $\mathbf{H_2L}Cl_2{\cdot}4H_2O$ (0.26 g, 0.5 mmol) was dissolved in mixture of water (15 mL) and acetonitrile (15 mL), then solid $Fe(BF_4)_2{\cdot}6H_2O$ (0.17 g, 0.55 mmol) was added. After complete dissolution of $Fe(BF_4)_2{\cdot}6H_2O$ in the reaction mixture solid NaN_3 (0.13 g, 2.00 mmol) was added. The reaction solution was heated to reflux and stirred for 2 h. After slow evaporation of solvent in a refrigerator (≈ 4 °C) for one week, bordeaux red crystals were obtained. Yield 0.11 g (37 %). IR: $\tilde{\nu}$ = 3546 (m), 3353 (m), 3081 (w), 3050 (w), 2966 (w), 2034 (s), 1613 (w), 1559 (m), 1518 (w), 1480 (w), 1404 (m), 1332 (m),1269 (w), 1202 (w), 1152 (w), 1054 (m), 971 (w), 911 (w), 808 (w), 745 (w), 682 (w), 655 (w), 522 (w) cm^{-1}; MS (ESI): *m/z* calcd. for $C_{19}H_{31}N_7O_2Fe(N_3)_2$: 529.2068, found 529.2068; elemental analysis calcd. (%) for $C_{19}H_{31}BFeF_4N_{13}O_2$: C 37.03, H 5.07, N 29.55; found C 36.96, H 5.11, N 29.59.

Synthesis of Cu(II) Complex (4): The ligand $\mathbf{H_2L}Cl_2{\cdot}4H_2O$ (0.26 g, 0.5 mmol) was dissolved in mixture of water (15 mL) and acetonitrile (15 mL), then solid $Cu(BF_4)_2{\cdot}6H_2O$ (0.12 g, 0.5 mmol) was added. After complete dissolution of $Cu(BF_4)_2{\cdot}6H_2O$ in the reaction mixture, solid NaN_3 (0.13 g, 2.00 mmol) was added. The reaction solution was heated to reflux and stirred for 2 h. After slow evaporation of solvent in a refrigerator (≈ 4 °C) for two weeks, deep green crystals were obtained. Yield 0.10 g (33 %). IR: $\tilde{\nu}$ = 3558 (m), 3356 (m), 3049 (w), 1651 (m), 1609 (s),1552 (s), 1524 (m), 1483 (s), 1440 (m), 1413 (m), 1382 (m), 1345 (w), 1271 (m), 1231 (w), 1206 (w), 1037 (s), 917 (m), 812 (w), 732 (w), 689 (w), 647 (w), 523 (w) cm^{-1}; MS (ESI): *m/z* calcd. for $C_{19}H_{31}N_7O_2CuBF_4$: 539.1859, found 539.1862; elemental analysis calcd. (%) for $C_{19}H_{35}B_2CuF_8N_7O_4$: C 34.44, H 5.32, N 14.80; found C 34.48, H 5.29, N 14.77.

X-ray Structure Determination

Crystal data and refinement parameters of compounds **1**–**4** are listed in Table 3. X-ray intensity data were collected at room temperature for **1**–**3** and at 150 K for **4** with Agilent SuperNova dual source diffractometer with an Atlas detector equipped with mirror-monochromated Mo-K_α radiation (λ = 0.71073 Å). The data were processed using CRYSALIS PRO.[61] The structures were solved by direct methods (SIR-92[62]) and refined by a full-matrix least-squares procedure based on F^2 using SHELXL-2016.[63] All non-hydrogen atoms were refined anisotropically. The water hydrogen atoms were located in a difference map and refined with the distance restraints (DFIX) with O–H = 0.96 Å and with $U_{iso}(H) = 1.5U_{eq}(O)$. All other hydrogen atoms were included in the model at geometrically calculated positions and refined using a riding model.

The *ORTEP*-3 for Windows[64] and *MERCURY*[65] programs were used for graphical presentations of the structures. The geometric parameters have been calculated using the program *PLATON*.[66]

Deposition Numbers 1994006 (for **1**), 1994007 (for **2**), 1994008 (for **3**), and 1994009 (for **4**) contain the supplementary crystallographic data for this paper. These data are provided free of charge by the joint Cambridge Crystallographic Data Centre and Fachinformationszentrum Karlsruhe Access Structures service www.ccdc.cam.ac.uk/structures.

Acknowledgments

This work was supported by the Ministry of Education, Science and Technological development of the Republic of Serbia (Grant OI 172055). We thank the Slovenian Research Agency (ARRS) through program P-0175 for financial support and EN-FIST Centre of Excellence, Dunajska 156, 1000 Ljubljana, Slovenia, for using SuperNova diffractometer. Marko Stojičkov acknowledge the support of ERASMUS + program. Andreas

Table 3. Crystal data and structure refinement details for **1**, **2**, **3**, and **4**.

	1	**2**	**3**	**4**
Formula	C19H35B2CoF8N7O4	C19H35B2F8N7O4Zn	C19H33BF4FeN13O3	C19H35B2CuF8N7O4
Fw [g mol^{-1}]	658.09	664.53	634.24	662.70
Crystal size [mm]	1.00×0.15×0.15	0.50× 0.20×0.10	0.80× 0.20× 0.10	0.70× 0.70× 0.10
Crystal color	red	yellow	red	green
Radiation, wavelength [Å]	Mo-K_α, 0.71073	Mo-K_α, 0.71073	Mo-K_α, 0.71073	Mo-K_α, 0.71073
Crystal system	monoclinic	monoclinic	orthorhombic	monoclinic
Space group	P 2/*n*	P 2/*n*	P b c a	P 2/c
a [Å]	6.2859(3)	6.3112(6)	9.9551(3)	18.6597(6)
b [Å]	19.7953(11)	19.7642(11)	14.7484(4)	11.8330(4)
c [Å]	11.6705(8)	11.6717(9)	38.4399(10)	12.5742(4)
β (°)	101.139(6)	100.869(8)	90.00	94.972(3)
V [Å3]	1424.82(14)	1429.76(19)	5643.8(3)	2765.94(16)
Z	2	2	8	4
Calcd density [g cm^{-3}]	1.534	1.544	1.493	1.591
F(000)	678	684	2632	1364
No. of collected reflns	7295	7456	51587	17527
No. of independent reflns	3273	3290	6451	6340
Rint	0.0259	0.0368	0.0435	0.0325
No. of reflns observed	2664	2525	5352	5425
No. parameters	198	198	384	390
R [$I > 2\sigma$ (I)][a]	0.0481	0.0494	0.0557	0.0473
wR_2 (all data)[b]	0.1319	0.1401	0.1695	0.1135
Goof, S[c]	1.033	1.062	1.069	1.090
Max./min. residual electron density (e/Å^3)	+0.61/–0.52	+0.66/–0.46	+0.73/–0.67	+0.90/–0.76

[a] $R = \Sigma||F_o| - |F_c||/\Sigma|F_o|$. [b] $wR_2 = \{\Sigma[w(F_o^2 - F_c^2)^2]/\Sigma[w(F_o^2)^2]\}^{1/2}$. [c] $S = \{\Sigma[w(F_o^2 - F_c^2)^2]/(n/p)\}^{1/2}$ where n is the number of reflections and p is the total number of parameters refined.

Scheitler thanks the DFG for the support through the IV 80/13-1project. Dušanka Radanović acknowledges financial support by the Ministry of Education, Science and Technological Development of the Republic of Serbia (Grant No. 451-03-68/2020-14/200026). Furthermore, we thank D. Blaumeiser for assistance and analysis of the IR spectroscopy measurements as well as Prof. Dr. M. Halik for providing the IR spectrophotometer. Open access funding enabled and organized by Projekt DEAL.

Keywords: Cobalt · Copper · Iron · Electrochemistry · SOD activity · Structure elucidation

[1] R. Pedrido, A. M. González-Noya, M. J. Romero, M. Martínez-Calvo, M. Vázquez López, E. Gómez-Fórneas, G. Zaragoza, M. R. Bermejo, *Dalton Trans.* **2008**, 6776–6787.
[2] I. Ivanović-Burmazović, K. Andjelković, *Adv. Inorg. Chem.* **2004**, *55*, 315–360.
[3] M. Regueiro-Figueroa, L. M. P. Lima, V. Blanco, D. Esteban-Gomez, A. de Blas, T. Rodriguez-Blas, R. Delgado, C. Platas-Iglesias, *Inorg. Chem.* **2014**, *53*, 12859–12869.
[4] S. Naskar, D. Mishra, S. Kumar Chattopadhyay, M. Corbella, A. J. Blake, *Dalton Trans.* **2005**, 2428–2435.
[5] C. Pichon, B. Elrez, V. Béreau, C. Duhayon, J.-P. Sutter, *Eur. J. Inorg. Chem.* **2018**, 340–348.
[6] Y. A. Tyula, A. Zabardasti, H. Goudarziafshar, M. S. Roudsari, M. Dusek, V. Eigner, *J. Mol. Struct.* **2017**, *1150*, 383–394.
[7] A. K. Bar, N. Gogoi, C. Pichon, D. P. Goli, M. Thlijeni, C. Duhayon, N. Suaud, N. Guihéry, A.-L. Barra, S. Ramasesha, J.-P. Sutter, *Chem. Eur. J.* **2017**, *23*, 4380–4396.
[8] M. U. Anwar, K. V. Shuvaev, L. N. Dawe, L. K. Thompson, *Inorg. Chem.* **2011**, *50*, 12141–12154.
[9] X.-C. Huang, C. Zhou, D. Shao, X.-Y. Wang, *Inorg. Chem.* **2014**, *53*, 12671–12673.
[10] L. Ratjen, J.-M. Lehn, *RSC Adv.* **2014**, *4*, 50554–50557.
[11] M. Dey, S. Dutta, B. Sarma, R. C. Deka, N. Gogoi, *Chem. Commun.* **2016**, *52*, 753–756.
[12] A. K. Mondal, A. Mondal, B. Dey, S. Konar, *Inorg. Chem.* **2018**, *57*, 9999–10008.
[13] L. J. Batchelor, M. Sangalli, R. Guillot, N. Guihery, R. Maurice, F. Tuna, T. Mallah, *Inorg. Chem.* **2011**, *50*, 12045–12052.
[14] C. Gökçe, N. Dilek, R. Gup, *Inorg. Chim. Acta* **2015**, *432*, 213–220.
[15] N. C. Kasuga, K. Sekino, M. Ishikawa, A. Honda, M. Yokoyama, S. Nakano, N. Shimada, C. Koumo, K. Nomiya, *J. Inorg. Biochem.* **2003**, *96*, 298–310.
[16] K. Anđelković, M. R. Milenković, A. Pevec, I. Turel, I. Z. Matić, M. Vujčić, D. Sladić, D. Radanović, G. Brađan, S. Belošević, B. Čobeljić, *J. Inorg. Biochem.* **2017**, *174*, 137–149.
[17] G.-F. Liu, M. Filipović, F. W. Heinemann, I. Ivanović-Burmazović, *Inorg. Chem.* **2007**, *46*, 8825–8835.
[18] D. Salvemini, Z. Q. Wang, J. L. Zweier, A. Samouilov, H. Macarthur, T. P. Misko, M. G. Currie, S. Cuzzocrea, J. A. Sikorski, D. P. Riley, *Science* **1999**, *286*, 304–306.
[19] D. P. Riley, O. F. Schall, *Adv. Inorg. Chem.* **2006**, *59*, 233–263.
[20] D. Lieb, F. C. Friedel, M. Yawer, A. Zahl, M. M. Khusniyarov, F. W. Heinemann, I. Ivanović-Burmazović, *Inorg. Chem.* **2013**, *52*, 222–236.
[21] D. Lieb, I. Kenkel, J. Miljkovic, D. Moldenhauer, N. Weber, M. R. Filipovic, F. Gröhn, I. Ivanović-Burmazović, *Inorg. Chem.* **2014**, *53*, 1009–1020.
[22] G. F. Kelso, A. Maroz, H. M. Cocheme, A. Logan, T. A. Prime, A. V. Peskin, C. C. Winterbourn, A. M. James, M. F. Ross, S. Brooker, C. M. Porteous, R. F. Anderson, M. P. Murphy, R. A. Smith, *Chem. Biol.* **2012**, *19*, 1237–1246.
[23] I. Batinic-Haberle, J. S. Reboucas, I. Spasojevic, *Antioxid. Redox Signaling* **2010**, *13*, 877–918.
[24] I. Batinic-Haberle, A. Tovmasyan, I. Spasojevic, *Redox Biol.* **2015**, *5*, 43–65.
[25] I. Spasojevic, I. Batinic-Haberle, J. S. Reboucas, Y. M. Idemori, I. Fridovich, *J. Biol. Chem.* **2003**, *278*, 6831–6837.
[26] J. S. Reboucas, I. Spasojevic, D. H. Tjahjono, A. Richaud, F. Mendez, L. Benove, I. Batinic-Haberle, *Dalton Trans.* **2008**, 1233–1242.
[27] Y. Sheng, I. A. Abreu, D. E. Cabelli, M. J. Maroney, A. F. Miller, M. Teixeira, J. S. Valentine, *Chem. Rev.* **2014**, *114*, 3854–3918.
[28] A. Haber, Z. Gross, *Chem. Commun.* **2015**, *51*, 5812–5827.
[29] H. Y. Ching, I. Kenkel, N. Delsuc, E. Mathieu, I. Ivanović-Burmazović, C. J. Policar, *J. Inorg. Biochem.* **2016**, *160*, 172–179.
[30] A. Fragoso, R. Cao, V. T. D'Souza, *J. Carbohydr. Chem.* **1997**, *16*, 171–180.

[31] I. Ivanović-Burmazović, M. S. A. Hamza, R. van Eldik, *Inorg. Chem.* **2002**, *41*, 5150–5161.
[32] D. Sarauli, R. Meier, G.-F. Liu, I. Ivanović-Burmazović, R. van Eldik, *Inorg. Chem.* **2005**, *44*, 7624–7633.
[33] M. R. Milenković, B. Čobeljić, K. Anđelković, I. Turel, *Eur. J. Inorg. Chem.* **2018**, 838–846.
[34] L. S. Vojinović-Ješić, V. I. Češljević, G. A. Bogdanović, V. M. Leovac, K. M. Szécsényi, V. Divjaković, M. D. Joksović, *Inorg. Chem. Commun.* **2010**, *13*, 1085–1088.
[35] G. Brađan, B. Čobeljić, A. Pevec, I. Turel, M. Milenković, D. Radanović, M. Šumar-Ristović, K. Adaila, M. Milenković, K. Anđelković, *J. Coord. Chem.* **2016**, *69*, 801–811.
[36] G. Brađan, A. Pevec, I. Turel, I. N. Shcherbakov, M. Milenković, M. Milenković, D. Radanović, B. Čobeljić, K. Anđelković, *J. Coord. Chem.* **2016**, *69*, 2754–2765.
[37] See ref.[16].
[38] K. Anđelković, I. Ivanović, B. V. Prelesnik, V. M. Leovac, D. Poleti, *Polyhedron* **1996**, *15*, 4361–4366.
[39] K. Andjelković, I. Ivanović, S. R. Niketić, B. Prelesnik, V. M. Leovac, *Polyhedron* **1997**, *16*, 4221–4228.
[40] I. Ivanović-Burmazović, A. Bacchi, G. Pelizzi, V. M. Leovac, K. Andjelković, *Polyhedron* **1998**, *18*, 119–127.
[41] A. W. Addison, T. N. Rao, J. Reedijk, J. van Rijn, G. C. Verschoor, *J. Chem. Soc., Dalton Trans.* **1984**, *7*, 1349–1356.
[42] A. H. Reath, J. W. Ziller, C. Tsay, A. J. Ryan, J. Y. Yang, *Inorg. Chem.* **2017**, *56*, 3713–3718.
[43] M. Manzanera-Estrada, L. F. H. Ayala, G. Osorio-Monreal, J. C. García-Ramos, L. Ortiz-Frade, *J. Mex. Chem. Soc.* **2013**, *57*, 192–197.
[44] F. C. Friedel, D. Lieb, I. Ivanović-Burmazović, *J. Inorg. Biochem.* **2012**, *109*, 26–32.
[45] I. Ivanović-Burmazović, M. R. Filipović, *Adv. Inorg. Chem.* **2012**, *64*, 53–95.
[46] I. Ivanović-Burmazović, *Adv. Inorg. Chem.* **2008**, *60*, 59–100.
[47] I. Ivanović-Burmazović, R. van Eldik, *Dalton Trans.* **2008**, *39*, 5259–5275.
[48] Y. Sheng, E. B. Gralla, M. Schumacher, D. Cascio, D. E. Cabelli, J. S. Valentine, *Proc. Natl. Acad. Sci. USA* **2012**, *109*, 14314–14319.
[49] A. S. Hearn, C. Tu, H. S. Nick, D. N. Silverman, *J. Biol. Chem.* **1999**, *274*, 24457–24460.
[50] I. A. Abreu, D. E. Cabelli, *Biochim. Biophys. Acta* **2010**, *1804*, 263–274.
[51] A. Franke, A. Scheitler, I. Kenkel, R. Lippert, A. Zahl, D. Balbinot, N. Jux, I. Ivanović-Burmazović, *Inorg. Chem.* **2019**, *58*, 9618–9630.
[52] R. Brigelius, R. Spöttl, W. Bors, E. Lengfelder, M. Saran, U. Weser, *FEBS Lett.* **1974**, *47*, 72–75.
[53] D. Klug-Roth, J. Rabani, *J. Phys. Chem.* **1976**, *80*, 588–591.
[54] N. Ségaud, E. Anxolabéhère-Mallart, K. Sénéchal-David, L. Acosta-Rueda, M. Robert, F. Banse, *Chem. Sci.* **2015**, *6*, 639–647.
[55] K. Dürr, B. P. Macpherson, R. Warratz, F. Hampel, F. Tuczek, M. Helmreich, N. Jux, I. Ivanović-Burmazović, *J. Am. Chem. Soc.* **2007**, *129*, 4217–4228.
[56] I. Kenkel, Biomimetic iron and manganese centers and their reactions with small molecules: Biomimetische Eisen- und Mangan-Zentren und ihre Reaktion mit kleinen Molekülen, PhD Thesis, Friedrich-Alexander University Erlangen-Nürnberg, Germany, **2017**.
[57] M. E. Aliaga, D. Andrade-Acuña, C. López-Alarcón, C. Sandoval-Acuña, H. J. Speisky, *J. Inorg. Biochem.* **2013**, *129*, 119–126.
[58] A. Fihri, V. Artero, A. Pereira, M. Fontcave, *Dalton Trans.* **2008**, 5567–5569.
[59] T. Sato, Y. Hamada, M. Sumikawa, S. Araki, H. Yamamoto, *Ind. Eng. Chem. Res.* **2014**, *53*, 19331–19337.
[60] S. V. Kryatov, E. V. Rybak-Akimova, S. Schindler, *Chem. Rev.* **2005**, *105*, 2175–2226.
[61] Oxford Diffraction, *CrysAlis PRO*, Oxford Diffraction Ltd., Yarnton (England), **2009**.
[62] A. Altomare, G. Cascarano, C. Giacovazzo, A. Guagliardi, *J. Appl. Crystallogr.* **1993**, *26*, 343–350.
[63] G. M. Sheldrick, *Acta Crystallogr., Sect. C* **2015**, *71*, 3–8.
[64] L. J. Farrugia, *J. Appl. Crystallogr.* **2012**, *45*, 849–854.
[65] C. F. Macrae, P. R. Edgington, P. McCabe, E. Pidcock, G. P. Shields, R. Taylor, M. Towler, J. van de Streek, *J. Appl. Crystallogr.* **2006**, *39*, 453–457.
[66] A. L. Spek, *ActaCrystallogr., Sect. D* **2009**, *65*, 148–155.

Received: April 30, 2020